Functionalized Basalt Scales by Green Method for Higher Performance of Anticorrosion Coatings

Yichao Guo[1] · Tianyue Jia[1] · Jingsha Tan[1] · Bo Zhang[1] · Honglei Guo[1] · Zhiyuan Feng[1] · Bing Lei[1] · Ping Zhang[2] · Guozhe Meng[1]

Abstract

In this study, basalt scales were activated by air plasma and were subsequently deposited with cerium dioxide nanoparticles to obtain CeO_2-modified basalts (CB). Inspired by mussel biomimetics, polydopamine (PDA) and 3-glycidoxypropyltrimethoxysilane were further employed to modify the properties of CB to obtain functionalized basalt scales (CBD). This treatment greatly increased the interfacial compatibility between inorganic fillers and epoxy resin. At the same time, PDA can form chelates with iron ions in the anodic area to prevent further corrosion. Tensile, water absorption, and electrochemical impedance spectrum measurements showed that incorporating CBD into epoxy resins resulted in the composite coatings with higher mechanical properties, water penetration resistance, corrosion resistance, and lower wetting properties.

Keywords Coating · Basalts scales · Air plasma · Corrosion resistance

1 Introduction

Offshore facilities and equipment, such as oil jacket platforms and vessels, will inevitably suffer from serious corrosion in marine environment [1–3]. Anticorrosive organic coating is one of the most commonly adopted protective measures, but its service life is difficult to achieve the expected target [4–6]. In order to improve the service life, inorganic lamellar fillers, which are excellent barrier to corrosive medium, are often added in the coating to form a lamellar organic "brick wall" structure [7]. The strong interaction between the interfaces of fillers and polymer matrix can provide ordered layered structures with an improved adhesion and integrity [8]. For example, Jing et al. prepared a new two-dimensional hybrid filler by hydrothermal

method, loaded ZrO_2 on the surface of PDA-modified MoS_2, and functionalized it with KH560. Adding filler to epoxy resin greatly improves the mechanical properties and corrosion resistance of the coating [9]. Moreover, the modification of fillers or cross-linking of polymer matrix can reduce the natural capillarity at the interface between filler and polymer, hindering the transport of O_2 and H_2O molecules through these capillaries, leading to enhanced corrosion protection [10, 11]. Therefore, selection of suitable fillers is an effective measure to improve the corrosion resistance and service life of the coating.

Basalt scales material as filler, which is mainly composed of silica (45–60 wt%), calcium oxide (6–12 wt%), and iron oxide (5–15 wt%) [12], is a low price material with excellent mechanical, acid, and alkali resistance [13, 14], and can serve as a barrier to water (labyrinth effect). But their compatibility and dispersibility in polymer matrix are poor due to their much higher surface energies than polymer matrices, smooth surfaces, and chemical inertness [15, 16]. This leads to premature degradation of coatings such as loss of adhesion, decline of shielding performance, and deterioration of mechanical properties. Therefore, surface modification of basalt scales to enhance their interfacial properties is an important research area. Luo et al. used 3 ‰ nano-SiO_2 microspheres to modify epoxy coatings containing basalt fillers, and the results showed that the modification could

✉ Guozhe Meng
menggzh3@mail.sysu.edu.cn

1   Marine Corrosion and Protection Team, School of Chemical Engineering and Technology, Sun Yat-sen University, Zhuhai 519082, China

2   Department of Civil and Environmental Engineering, Faculty of Science and Technology, University of Macau, Taipa, Macau SAR, China

enhance coating chemical stability, water permeability, and mechanical properties [17]. Then, basalt scale fillers were subsequently modified by urinary aldehyde microspheres [18] and sulfonated aniline trimer to form chemical bonding (covalent grafting or hydrogen bond adsorption) [19] at coating/fillers interface, further enhancing the interfacial compatibility, corrosion resistance, and mechanical properties of the coating. Regarding smooth surfaces and high surface energy of basalt scales, Li et al. sequentially deposited polydopamine (PDA) and AgNP$_S$ on NaOH-etched basalt, which were added to epoxy resin to achieve good corrosion resistance and antibacterial properties [19]. The activation treatment of basalt scales is mostly concentrated acid and alkali etching, which is unsafe and environmentally unfriendly. Therefore, one can expect that high-performance anticorrosive coating can be prepared by adopting better basalt scale activation method and improving the interface combination of polymer coating/filler by covalently modifying basalt scale surface.

In this study, an environmentally friendly and facile protocol by air plasma treatment on basalt scales is adopted to realize surface activation of basalt fillers. Cerium dioxide particles are then deposited on the surface of basalt scales. After activation, the abundant Si–OH groups on the surface of basalt scales can enhance the interaction between the carrier and CeO_2, and promote the high dispersion of CeO_2 on the surface. And the rough surface enhances the mechanical occlusal ability of basalt scales and epoxy resins [20]. Furthermore, inspired by the strong adhesion of mussel, polydopamine with a strong adhesion ability was adopted to cover the surface of basalt scales, which greatly improved the settling property of basalt scales in epoxy resin. On the other hand, cerium dioxide and polydopamine can act as corrosion inhibitors to effectively control corrosion. Finally, 3-glycidoxypropyltrimethoxysilane (GPTMS) is grafted to achieve secondary functionalization of basalt scales. According to the similar miscibility principle, a large number of C chains and epoxy groups grafted improve the dispersion of basalt scales in epoxy resin. Investigations have been made on the addition of modified basalt scales to the epoxy coating and their anticorrosive performance.

2 Materials and Methods

2.1 Materials

Basalt scales (500 mesh) purchased from Yantai Huazheng Kexin New Material Technology Co. Ltd. (Yantai, China). Cerium nitrate hexahydrate was purchased from Adamas Reagent Co. Ltd. Urea was purchased from Shanghai Aladdin Biochemical Technology Co. Ltd. Dopamine hydrochloride and trimethylol aminomethane (Tris) were purchased from Shanghai Maclin Biochemical Technology Co. Ltd. All chemicals are used as without further purification. The metal base material was 5 cm×5 cm×1 mm Q235 carbon steel. After sandblasting, it was washed with acetone and anhydrous ethanol for degreasing and dehydration. Epoxy resin (E44, Nantong Xingxing Synthetic Materials Co. Ltd., China) and 650 polyamide curing agent (Dingyuan Danbao Resin Co. Ltd., China) (mass ratio 2:1) were used to prepare the coating. BYK-333 is a leveling agent.

2.2 Activation Treatment of Basalt Scales

Basalt scales (abbreviated as BS) (500 mesh) were selected as the research object in the experiment. Before use, they were washed with acetone and ethanol to be free of impurities and dried in a blast drying oven at 80 °C. In order to select the best activation method, the activation effect of several different basalt scales activation methods was compared. BS were activated by H_2SO_4, NaOH, H_2O_2, and air plasma, respectively.

BS (10.0 g) were added to a conical bottle containing 300-ml 2 M H_2SO_4 solution, heated to 100 °C, and stirred for 2 h (H_2SO_4 activation method [21], the samples were noted H_2SO_4-BS). BS (10.0 g) were added to a Teflon conical bottle with 4 M NaOH solution, heated to 100 °C, and stirred for 2 h (NaOH activation method [22], the samples were noted as NaOH-BS). BS (10.0 g) and hydrogen peroxide solution (40 g, 30%) were added to the 100-ml round-bottom flask, condensed and refluxed at 100 °C, and stirred for 2 h (H_2O_2 activation method [23], the samples were noted as H_2O_2-BS). BS (10.0 g) and deionized water (100 ml) were added to the autoclave under 15 MPa and were stirred at the speed of 600 r/min for 24 h. And the mixture was filtered and washed with deionized water severally until the solution pH was ~ 7. Then, the etched BS were dried in a vacuum drying at 60 °C for 12 h (high-pressure water activation method [24], the samples were noted as HP water-BS). BS (10.0 g) were put into a plasma treatment instrument, and its surface was treated with air for 1800 s (air plasma treatment, the samples were noted as P-BS).

2.3 Preparation of Modified Basalt Composites

The preparation scheme of fillers and coatings is shown in Fig. 1. Plasma-treated BS (P-BS, 10 g), 0.1 M cerium nitrate hexahydrate solution (10 ml), and 1 M urea solution (60 ml) were added to the beaker, respectively. Following this, the mixture was heated to 43 °C and maintained at this temperature for 30 min under stirring. Then, the above mixture was transferred to 100-ml hydrothermal reactor and reacted for 24 h at 100 °C. After the reaction was completed, it was naturally cooled to room temperature, and the sample was washed by centrifugation with deionized water and dried.
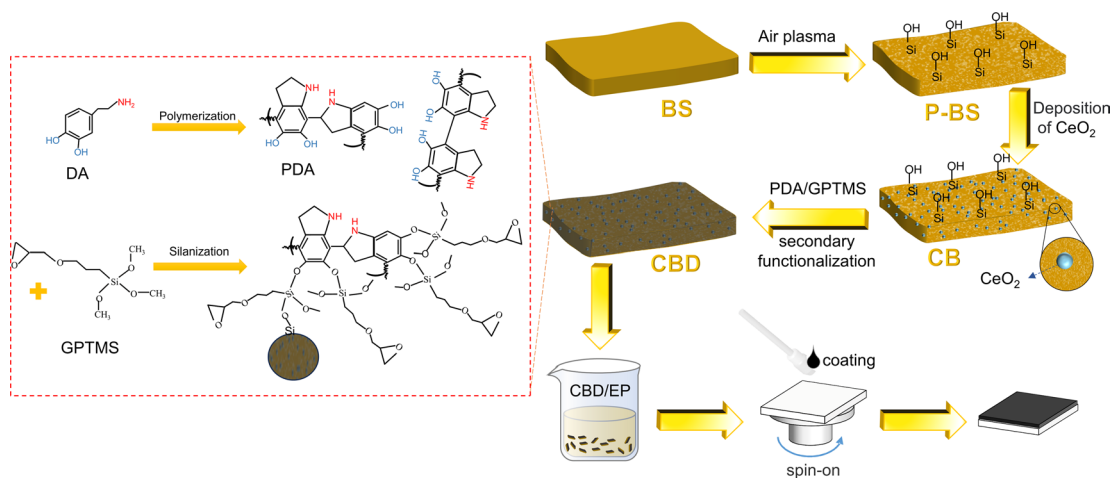
Fig. 1 Preparation technology of filler and coating

Finally, the dried samples were heat-treated in muffle furnace (air environment) at 350 °C for 4 h and then dried in vacuum at 80 °C to obtain basalt scales with CeO_2 deposited on the surface (the obtained samples are noted as CB).

Tris (0.2436 g) was dissolved in 200-ml deionized water, and dopamine hydrochloride (800 mg) was added to keep pH around 8.5. The synthesized CB was added and stirred for 15 h at 60 °C in above solution to form dopamine-coated samples. Then, the samples were filtered out, washed with deionized water, and dried at 60 °C.

A mixed solution of anhydrous ethanol and deionized water (the mass ratio of 9:1) was prepared, and GPTMS (1 ml) was added to the solution, hydrolyzed at room temperature for 1 h under stirring. The dopamine-coated samples were added to the solution, stirred for 2 h, centrifugated with deionized water and anhydrous ethanol, and then dried in vacuum at 60 °C for 12 h. The finally obtained samples were noted as CBD. The schematic illustration for the synthesis of CBD is displayed in Fig. 1.

2.4 Preparation of Anticorrosion Coatings

The epoxy resin (32 g) was dissolved in a mixture of leveling agent (0.06 g), xylene (6.72 g), and n–butanol (2.88 g). Then, BS, CB, and CBD (20 wt% of epoxy mass) were added, respectively, and stirred at a speed of 600 r/min for 1 h on a magnetic agitator. After the dispersion, add polyamide curing agent (16 g) and manually stir evenly to form different paintings. Then, these paintings were coated (by spin coating method) on Q235 carbon steel to form epoxy varnish coating (EP) as well as epoxy coatings containing BS, CB, and CBD (noted as BS/EP, CB/EP, and CBD/EP), respectively. Then, they were put into a vacuum drying oven vacuum defoaming until no continuous bubbles emerge. The coating thickness was controlled to 160 ± 5 μm by adjusting the rotating speed, time, and feeding times. After the coatings were prepared, they were left for 1 h, then the sample was placed in the oven and cured at 40 °C for 4 h, 60 °C for 24 h, and cured at room temperature for 7 days.

2.5 Characterization

The morphologies of the various fillers (BS, H_2SO_4-BS, NaOH-BS, H_2O_2-BS, P-BS, CB, and CBD) and the prepared coatings were characterized using a field emission scanning electron microscope (FESEM, Zeiss Sigma 300, Japan), and the composition of the surfaces was analyzed by the energy-dispersive X-ray spectrum (EDS). High-definition CCD microscope (KSGAOP IN, China) was used to analyze the surface morphology of stator and matrix after dry and wet adhesion test.

Fourier transform infrared spectrometer (FT-IR, Perkin-Elmer Spectrum Two, USA) was used to analyze the change of functional groups before and after the modification of fillers. The KBr pellets were used, and the analysis was performed in the wavenumber range 450–4000 cm^{-1}. The graft amount of filler was assessed on thermogravimetric analysis with 10 °C/min of heating rate, in the range of 30–800 °C, under N_2 atmosphere (TG, Q500 TA).

The crystal structure of the inorganic fillers was determined by X-ray diffraction (XRD, Ultima IV, Japan) using the "Cu *K*" radiation source in the angle range 10–80° at a scanning rate of 10° min^{-1}. The dispersion of the fillers in the epoxy coating was characterized using the sedimentation test. The basalt scales were added into the epoxy coating without curing agent, ultrasonic for 30 min, and collected into the sample bottle. Then, the sample bottle was placed in the camera system device, and the Canon EOS camera was used to take pictures at a regular interval of 10 min.

The coating adhesion with the substrate was characterized using instrument of pull off adhesion (DeFelsko Posi Test, USA). The tests were carried out after immersing the samples in 3.5 wt% NaCl solution for 0 h and 1440 h at room temperature. The mechanical properties of the composite coatings were characterized by using an electric universal testing machine (AGX-V, 50N, China). An extension rate of 2 mm/min was determined according to ISO 37–2005 [25]. The static water droplets (2 µl) CA values were the mean values of five measurements obtained at different positions using an Dataphysics-OCA 20 contact angle system (Dataphysics-OCA20, German) at ambient temperature.

The corrosion resistances of the coatings were characterized by monitoring the open-circuit potential and electrochemical impedance spectroscopy on electrochemical workstation (Princeton Applied, USA). The prepared samples (working electrode), platinum plate (counter electrode), and $Hg/HgCl_2$ (saturated KCl) (reference electrode) were set in an electrolytic cell containing about 300-ml NaCl solution (3.5 wt%), constituting conventional three–electrode cell. The coating samples had an exposure area of 4.9 cm^2. In the early stage of the test, the disturbance voltage was set to 50 mV, and after 60 days, it was changed to 20 mV. The electrochemical impedance spectrum (EIS) was measured in the frequency range of 10^{-2}–10^5 Hz. Moreover, the recorded EIS results were fitted by the ZSimpWin software to obtain detailed corrosion data. The electrolytic cell was placed in the Faraday cage during the testing. At least three parallel experiments were performed at the same time for all tests.

3 Results and Discussion

3.1 Activation Treatment of Basalt

The high-temperature preparation process of basalt results in a very small amount of hydroxyl groups on its surface [26] to activate basalt surface. The hydroxylation degree of BS by various methods was studied in terms of the peak intensity ratio of -OH/Si–O–Si with FT-IR. Figure 2a shows that the characteristic peaks of Si–O–Si in basalts are in the range of 850–1275 cm^{-1} [27]. Compared with BS sample, the samples (H_2SO_4-BS, NaOH-BS, H_2O_2-BS, and P-BS) have obvious stretching vibration signals of –OH near 3420 cm^{-1}, [28] indicating that the number of hydroxyl groups on the surface of basalts increases after activation. Interestingly, the sample treated by plasma has a new-OH signal around 1385 cm^{-1}. The ratio of the peak intensity of –OH/Si–O–Si was obtained (Table 1). According to the degree of hydroxylation, the activation methods were ranked as H_2SO_4 > NaOH > plasma > hydrogen peroxide > high-pressure water. Although the activation degree of plasma treatment is slightly smaller than that of H_2SO_4 treatment and NaOH treatment, plasma treatment is obviously more environmentally friendly and facile than the latter. On the other hand, the surface morphology of basalt scales after activation treatment is shown in Fig. 2b. After NaOH, H_2SO_4, and
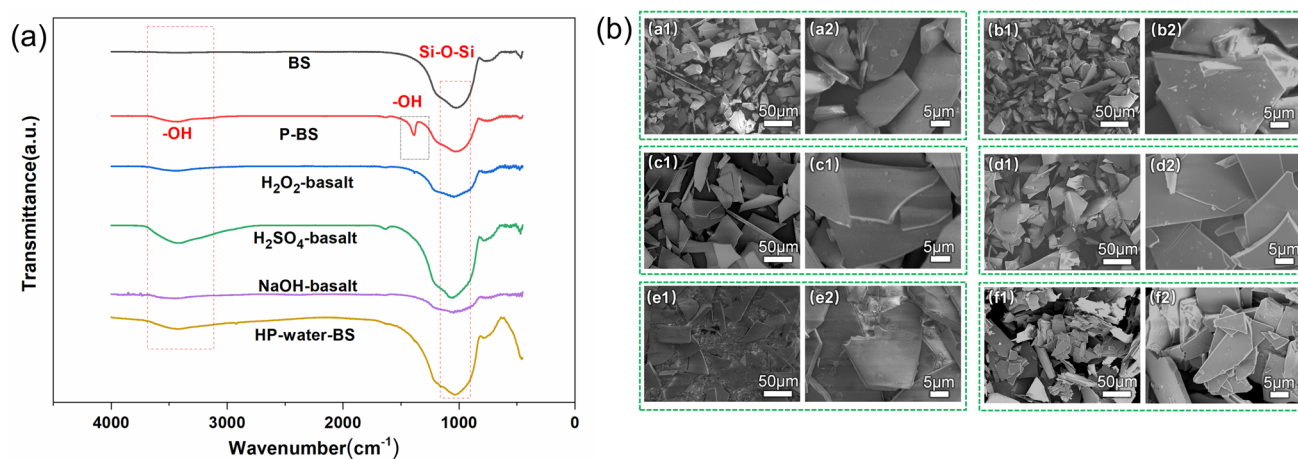

Fig. 2 **a** FT-IR of basalts treated by several activation methods. **b** SEM characterization of basalts activated by different methods: **a1**, **a2** BS; **b1**, **b2** P-BS; **c1**, **c2** H_2O_2-BS; **d1**, **d2** H_2SO_4-BS; **e1**, **e2** NaOH-BS; and **f1**, **f2** HP water-BS

Table 1 Hydroxyl ratio of basalt treated by several activation methods

Sample	BS	P-BS	H_2O_2-BS	H_2SO_4-BS	NaOH-BS	HP water-BS
–OH/Si–O–Si	0	0.1630	0.1548	0.2462	0.2236	0.1211

high-pressure water treatment, the size of basalts decreased, and the phenomenon of fracture was observed. Therefore, considering the influence of hydroxylation degree, easiness of operation, and material damage during processing, air plasma treatment of basalt was selected as the activation method for the following investigation on the P-BS sample.

3.2 Characterization of Basalt Modified by Cerium Dioxide and Polydopamine

As shown in Fig. 3a1 and a2, the surface of BS was quite smooth that it is difficult to achieve mechanical occlusion between basalt and epoxy resin, which is not conducive to the formation of a strong filler/resin interface. Therefore, the surface of P-BS needs to be further roughened. As shown in Fig. 3b1 and b2, a layer of rod-like CeO_2 nanoparticles was successfully deposited on the surface of basalt scales, and the size was about 100–200 nm. Due to the loading of CeO_2, the basalt changes from a smooth surface to a rough surface.

As shown in Fig. 3c1 and c2, a clear layer (maybe dopamine and GPTMS) can be observed on the surface of CBD sample, whose edge change from sharp to obtuse compared to Fig. 3a1, a2 and b1, b2, EDS characterization (Fig. 3d1) demonstrated that five elements (C, Al, Si, Ca, and Ce) could be identified on the surface of CBD sample. As shown in Fig. 3e1 and e2, the contents of Al, Si, and Ca in modified basalts decreased significantly, the content of C element was greatly increased, and the content of cerium element was also increased moderately.

In order to study the changes of surface chemical functional groups of BS, the basalts before and after modification were characterized by infrared spectroscopy. The results of FT-IR (Fig. 4a) indicate that the basalts show symmetric and asymmetric stretching vibrational peaks of Si–O–Si in the range of 850–1275 cm^{-1} [28]. Besides, the peaks at 766 cm^{-1} and 562 cm^{-1} indicate the Si–O stretching and bending vibrations, respectively [29, 30]. Another characteristic peak at 466 cm^{-1} represents the Al–O stretching
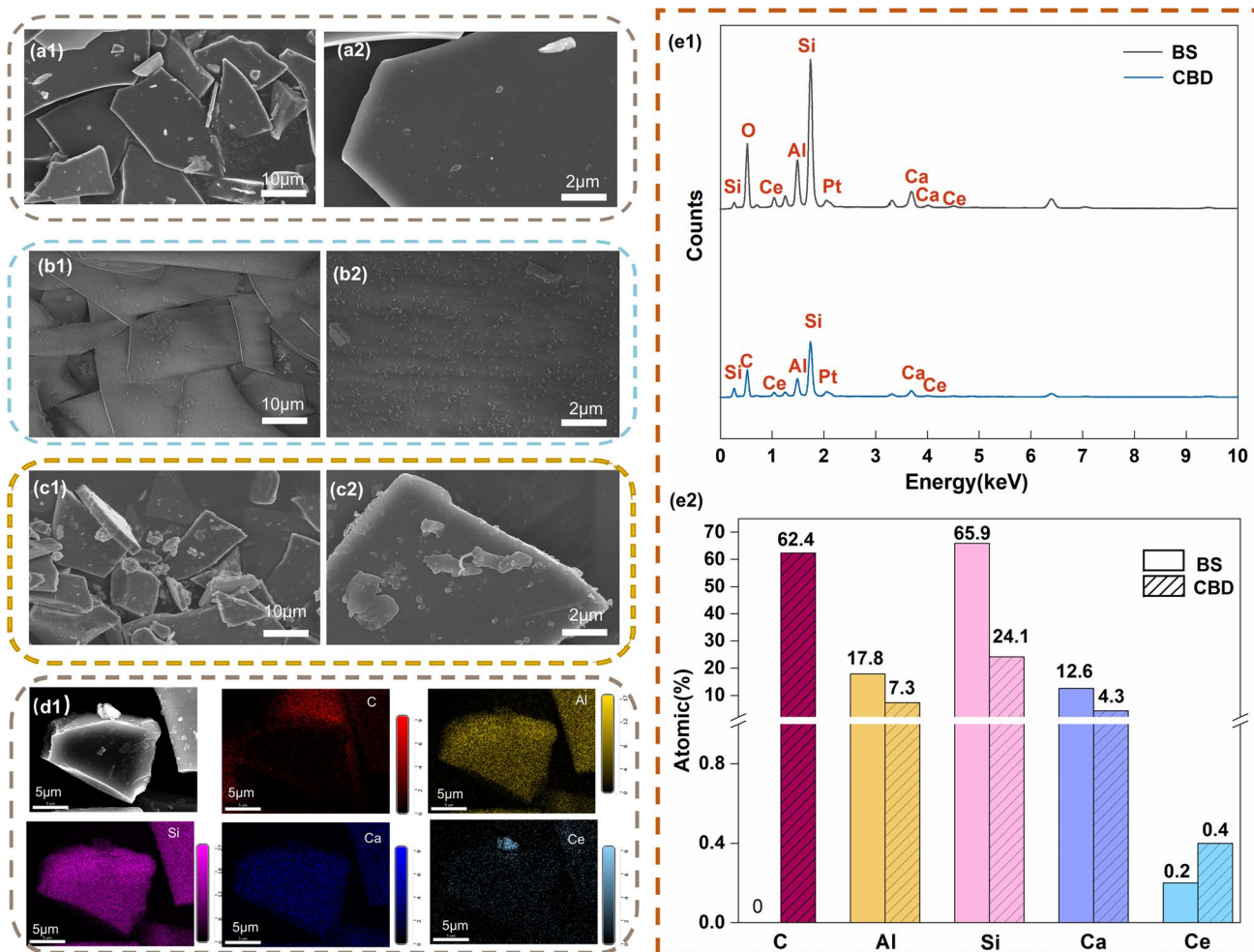

Fig. 3 SEM images of BS **a1**, **a2**; CB **b1**, **b2**; CBD **c1**, **c2**; EDS image of CBD **d1**; and variation diagram energy spectrum element content in modified basalt scales (CBD) compared with original basalt scales (BS) **e1**, **e2**
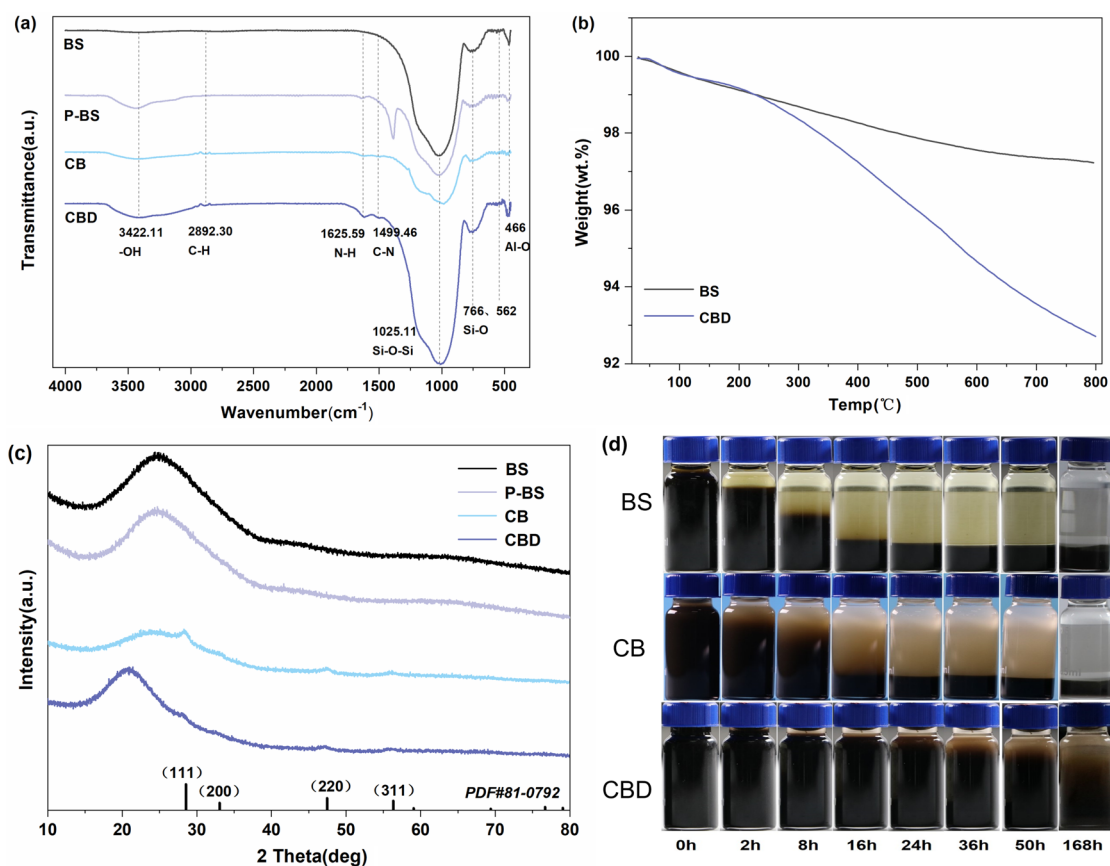
Fig. 4 **a** FT-IR pattern; **b** thermogravimetric analysis (TGA) pattern; **c** XRD pattern; **d** settlement behavior of BS; CB; and CBD in epoxy resin coatings

vibration [31]. In the spectra of the CBD hybrids, 1625.6, 2892.3, and 1499.5 cm^{-1} correspond to the stretching vibrations of N–H, C–H, and C–N, respectively [16, 18, 32]. The above information indicates the successful modification of basalt by PDA and GPTMS. In addition, the increase in Si–O–Si peak intensity also indicates that GPTMS has undergone dehydration condensation reaction with Si–OH on activated basalt scales.

The thermogravimetric properties of BS before and after modification were studied by TGA analysis. As shown in Fig. 4b, BS is stable at 0–800 °C, and the final mass loss was 2.76%, which may be due to the degradation and volatilization of impurities and water. The decomposition step of CBD is very large in the temperature range of 200–800 °C, and the final weight loss rate was up to 7.24%, which is mainly due to the degradation of PDA and GPTMS. The results show that at 800 °C, the residue of BS is about 4.5 wt% higher than that of CBD, suggesting that the load of PDA and GPTMS is about 4.5 wt%.

Figure 4c presents the XRD patterns of basalt and three kinds of modified basalt and the standard PDF card of CeO$_2$ (JCPDS# 65–2975). The unmodified basalt has a large inclusion peak at 2θ = 26°, indicating of a poor crystallinity,

which may be due to the heat treatment temperature of less than 700 °C during preparation. The sharp peaks of the CB and CBD hybrids at 2θ = 28.28°, 32.8°, 46.98°, and 55.8° correspond well to the characteristic peaks of the (111), (200), (220), and (311) crystal planes in the CeO$_2$ standard card, and the reflection peak intensity of the modified basalt is weakened, which also proves the successful coating of dopamine [33–35].

To analyze the interface compatibility of the basalt scales as well as the CB and CBD hybrids with the epoxy coating, sedimentation test was carried out to monitor the settlement behavior of basalt scales. For example, Zheng et al. prepared a new type of coating filler (BUF) via activating basalt scales by chemical etching and coating the etched scales with a layer of urea–formaldehyde microspheres. The compatibility between BUF filler and epoxy coating was analyzed by sedimentation experiment. The result was a slight precipitation of the BUF hybrid material after 120 h [18]. We increased the sedimentation test time to 168 h. Figure 4d shows the settling behavior of the three basaltic scales from 0 to 168 h. The unmodified basalt precipitates completely within 16 h, which indicates that the unmodified basalt is poorly dispersed in epoxy resin. Due to the deposition of

CeO$_2$ nanoparticles on the surface, the surface of the CB hybrid becomes rough, so the mechanical occlusal ability between the hybrid and epoxy resin is improved, and the dispersion performance is slightly better in the sedimentation test. Compared with BS and CB hybrids, CBD hybrids are very stable in epoxy resin, and there was only a small amount of precipitation within 50 h. Some fillers which are stably dispersed in epoxy resin could be observed even after 168 h. Due to the principle of similar substances dissolve each other, the surface of inorganic BS after secondary functionalization is grafted with a large number of C chains and epoxy groups with an enhanced the non-polarity. The interfacial compatibility with epoxy resin as well as the dispersion properties improved. The results of deposition test show that the plasma treatment and modification of BS can noticeably improve the interface compatibility between BS and coating matrix.

3.3 Physical Performance of Composite Coatings

3.3.1 Mechanical Properties of Composite Coatings

The strength and crack propagation behavior of the coating were investigated by tensile test. The stress–strain curves of Fig. 5a show the tensile strength of the three kinds of coatings (EP, BS/EP, and CBD/EP). It can be seen that they could all fracture after the yield point, indicating of the characteristics of ductile fracture. The CBD/EP coating shows the highest tensile strength (39.93 MPa), followed by EP (32.06 MPa), and the lowest is BS/EP (27.65 MPa) coatings. Apparently, the addition of unmodified BS cannot enhance the strength of the coatings (27.65 MPa),

which even decrease compared to EP coating (32.06 MPa). It may be due to the failure of the basalt to combine closely with the epoxy resin coating and produce more defects in the interior [36]. However, the mechanical riveting effect of cerium dioxide deposited on the surface of the filler (CB), as well as the possible strong chemical binding between dopamine and epoxy resin on CBD samples increase the tensile strength of the coating to 39.93 MPa. This is because the chemically bonded coating/filler interface can prevent the crack propagation of the polymer films [37–39].

Figure 5b–d shows the fracture micro-morphology after tensile test via the SEM images of the tensile sections of the coatings. Figure 5b1 and b2 shows the fracture morphology of pure epoxy coating, which is very smooth, and there were few internal defects in the coating. It can be seen that only a few cracks and a single fracture surface were formed, and the fracture morphology was similar to brittle fracture, indicating of its weak anti-crack propagation property. Figure 5c1 and c2 shows the fracture morphology of the BS/EP coating. There are many cracks along the interface between BS and epoxy resin, indicating of a weak bonding between fillers/epoxy. When the coating was subjected to tensile loading, these interfaces became the source of cracks and underwent rapid cracking, which, in turn, became a fast channel for the invasion of corrosive media, leading to a rapid deterioration of the coating's anticorrosion ability. For CBD/EP coating (Fig. 5d1 and d2), the number of cracks significantly decreased, and the interface was highly intact. Moreover, a large number of ductile dimples appeared near the interface and extended into river-like patterns, indicating that CBD not only enhances the tensile strength of the coating, but also significantly enhances the interfacial adhesion and
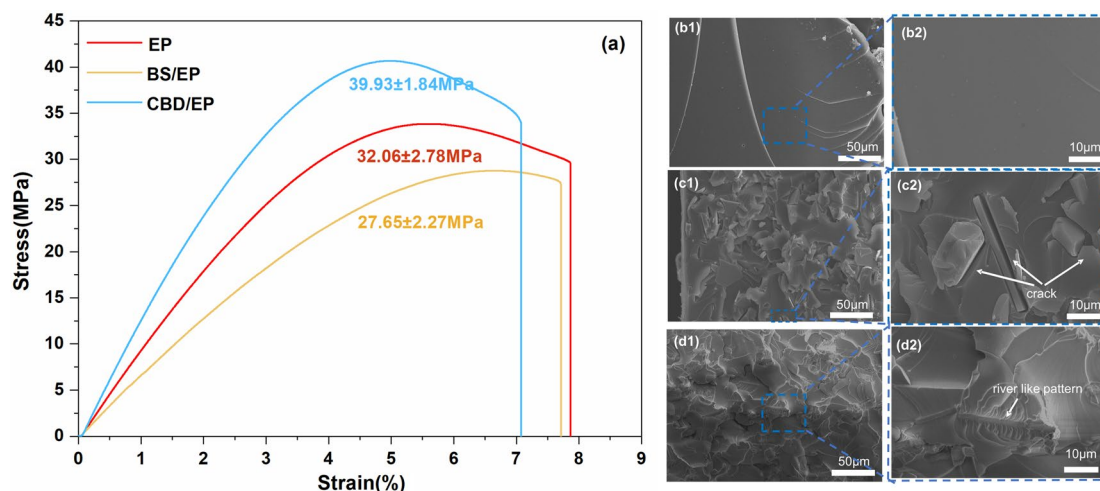

Fig. 5 Stress–strain results of EP, BS/EP, and CBD/EP coatings **a**; SEM images of the tensile sections of several coatings (EP, BS/EP, and CBD/EP) **b1**–**d2**

compatibility, which was manifested as brittle cracking of the coating and local ductile cracking near the interface.

3.3.2 Adhesion of Composite Coatings with Metal Substrates

Loss of adhesion between coating and metal is a major cause of coating failure [40]. Therefore, we tested the dry and wet (after 75 d immersion in 3.5 wt% NaCl) adhesion of these coatings, and calculated the adhesion loss ratio according to Eq. (1). The results are shown in Fig. 6a. It can be seen that the dry adhesion values of EP, BS/EP, and CBD/EP coatings are 6.16, 7.44, and 8.42 MPa, respectively. Among them, the adhesion value of CBD/EP coating is the highest, which may be due to the bonding among NH_2 of PDA, Si–OH of GPTMS, and the metal matrix, which enhances the coating/metal interface bonding strength. Besides, the wet adhesion is another key parameter affecting the coating performance [41]. After soaking in 3.5 wt% NaCl for 75 d, the coatings' adhesion decreased to 2.80, 4.26, and 7.02 MPa, respectively. After soaking, the adhesion of EP coating decreased significantly, and the adhesion loss was as high as 54.5%. The adhesion loss of the coatings with BS is all lower than that of the pure epoxy coatings. Among them, CBD/EP has the smallest adhesion loss (about 16.6%). Li et al. optimized an environmentally friendly rust removal and transformation agent based on tannic acid through orthogonal test, and evaluated the adhesion of epoxy coating system. After tannin conversion treatment, the adhesion of the coating system increased from 1.93 to 5.97 MPa [42]. In contrast, after soaking in 3.5% NaCl for 75 days, the adhesion of our prepared CBD/EP coating only decreased from 8.42 to 7.02 MPa, showing better adhesion with the substrate.

Adhesion loss

$$= \frac{\text{Dry adhesion strength} - \text{Wet adhesion strength}}{\text{Dry adhesion strength}} \times 100\%. \quad (1)$$

Figure 6b shows the macroscopic morphology of carbon steel and coating surfaces after adhesion pull-out tests under various conditions. The figure shows the detachment area of the surface coating on the carbon steel substrate and the surface morphology of the metal after drawing. From the figure, it can be found that the dry adhesion peeling area of the basalt samples is smaller than that of pure epoxy, among which the modified basalt (CBD/coating) has the smallest stripping area, which also proves that the interface strength is higher. After soaking in 3.5 wt% NaCl for 1800 h, the surface of carbon steel coated with EP coatings showed large area corrosion, and obvious corrosion products appeared. The carbon steel coated with BS/EP coatings also had obvious corrosion, while the carbon steel coated with CBD/EP coating only had slight corrosion, and no corrosion products were found on the surface. In conclusion, BS/EP coating can prevent corrosive particles from reaching the metal matrix due to the deposition of BS compounds at the bottom, which have excellent water shielding performance. For CBD/EP coating, due to the formation of enhanced chemical bond (Ce-O-metal) between the deposited CeO_2 and metal, and the secondary functionalized grafted PDA and GPTMS have a large amount of $–NH_2$ and Si–O, and will also form a bond with metal. Therefore, CBD can significantly improve the dry and wet adhesion of epoxy resin. In other words, the addition of CBD improves the bonding strength between epoxy resin and metal matrix.
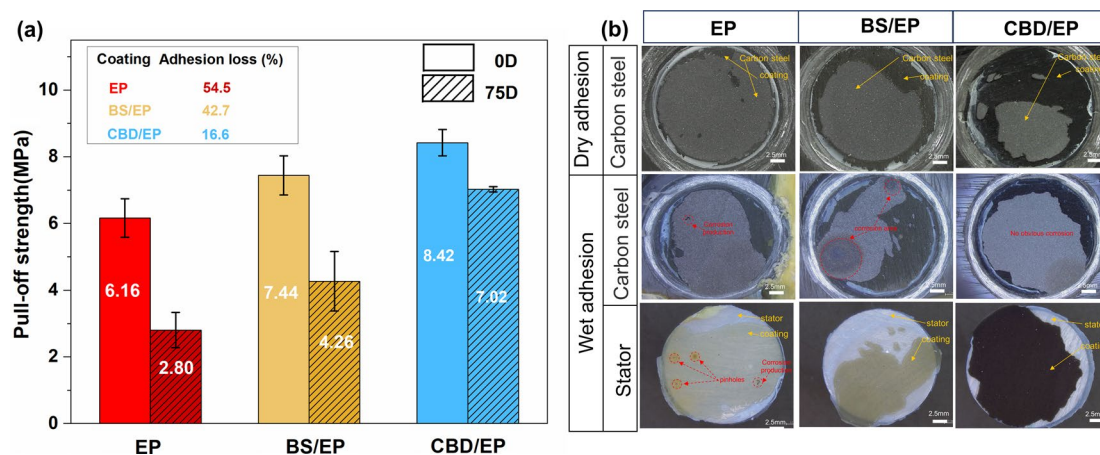

Fig. 6 Adhesion strengths of EP, BS/EP, and CBD/EP coatings before and after immersion in 3.5 wt% NaCl solution for 1440 h **a**. Visual illustration of the coating adhesion after testing **b**

3.3.3 Effect of Chemically Bond Between Coating/Filler Interface on Water Absorption Behavior

Contact angle is an important parameter used to quantify the wettability of solid surface [43]. Figure 7a shows the contact angle test results of EP, B/EP, and CBD/EP coatings. The addition of unmodified basalt to the epoxy coating reduces the contact angle, which may be due to the fact that the BS were concentrated in the lower layer, distributed unevenly, and bonded with epoxy resin in the form of physical bonding. There was a gap between the interface and this defect further became the path of water, leading to the deterioration of the surface properties of the composite coating. The hydrophobicity of CBD/EP coating is the best among the three samples, which may be due to the good dispersion of BS in the coating (Fig. 4d). In addition, BS have good hydrophobicity, and after surface secondary functionalization, the surface energy of BS becomes lower and enhances the interfacial bonding strength. At the same time, the addition of modified basalt scales reduces the stress concentration in the curing process of the coating, resulting in an increased contact angle.

The water absorption of the coating is considered to be the first stage of its failure, and high-pressure water absorption will have negative effects on the coating. For example, water adsorption will cause cracking, peeling, and blistering, which will lead to the failure of the coating on the metal substrate [44, 45]. In order to further study the water absorption of the modified coating, the water absorption of the coating was tested, and the test results are shown in Fig. 7b. We can observe that the water absorption behavior of the three kinds of coatings increased linearly in the initial stage, and the water absorption was gradually saturated with immersion time. In this stage, the water absorption rate of EP coating was the highest, followed by BS/EP and CBD/EP coatings. For saturated water absorption stage, EP coating is still the highest, which is about 1.52%, followed by BS/EP (0.89%) and CBD/EP (0.81%) coatings. The addition of BS greatly reduced the water absorption rate and saturated water absorption of the coating by the formation of "labyrinth effect" [44, 46]. In addition to the traditional "labyrinth effect" of BS that blocks the transmission of water in the coating, there should also be other mechanisms of action for modified BS. For the deposition of CeO_2, stronger mechanical riveting bonding force will reduce the diffusion channels of water formed by interface cracks. On this basis, the secondary surface modification of dopamine/GPTMS not only further enhanced the binding force between BS/EP (Fig. 5c1 and c2), but also enhanced the non-polarity of the coating near the interface by chemical bonding between dopamine ($–NH_2$) and EP polar functional groups (epoxy group), endowing the coating with stronger hydrophobic properties and making water transport more difficult in the coating.
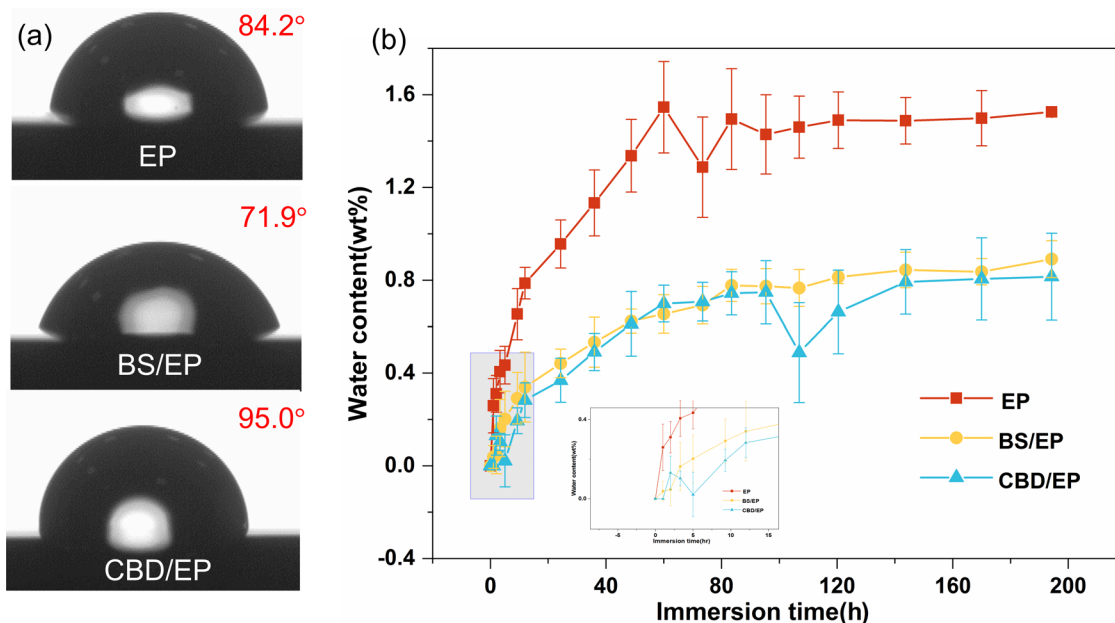

Fig. 7 Contact angles of water droplets (2 μL) on EP; BS/EP; and CBD/EP coatings **a**. Water absorption of different coatings **b**

3.4 Corrosion Resistance of Composite Coatings

3.4.1 Open-Circuit Potential (OCP) Measurements

The OCP values of the EP, BS/EP, and CBD/EP coatings were measured in the open-circuit state (Fig. 8). The open-circuit potential of all samples decreased in a fluctuating manner, with the potential fluctuations of EP and BS/EP samples being greater, while the fluctuations of CBD/EP were the smallest. After 155 days of immersion, the corrosion potential of CBD/EP can still maintain its highest value, while the potentials of other samples have already significantly decreased. During the immersion process of 0–35 days (decreasing rapidly), the OCP values of EP, BS/EP, and CBD/EP coatings decreased to 216.179, −290.8, and −134.289 mV, respectively. This shows that the corrosive medium diffuses rapidly in the coating matrix, which leads to the decrease in OCP value [47, 48]. The sudden increase and decrease in OCP values of EP and BS/EP coatings in the middle may be due to the fact that corrosion products or resin swelling block the entry channel of corrosive media. After 155 days of soaking, the OCP value of CBD/EP coating was −87.64 mV, which was higher than that of EP (−171.185 mV) and BS/EP coatings (−652.218 mV). The overall results of OCP values show that CBD/EP coating has a better anticorrosive performance in 155 days test.

3.4.2 EIS Measurements

The corrosion resistance of the coatings was studied by the EIS analysis conducted in 3.5 wt% NaCl solution. Figure 9 shows the results of the Bode and Nyquist diagrams of EP,
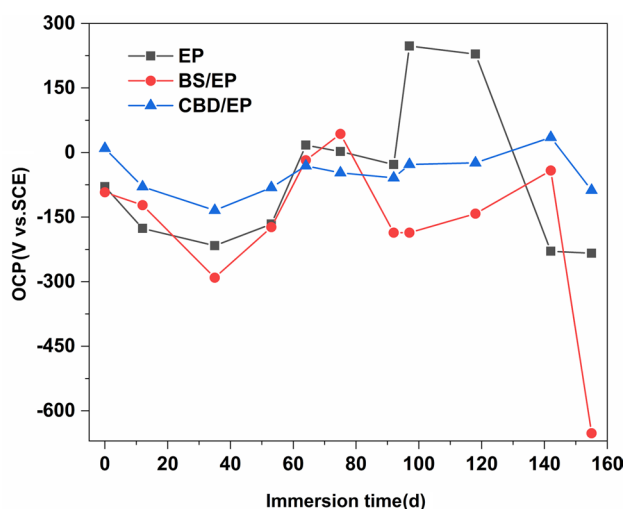

Fig. 8 Open-circuit potential (OCP) values of EP, BS/EP, and CBD/EP coatings after different periods of immersion in 3.5 wt% NaCl solution

BS/EP, and CBD/EP coatings, as well as the corresponding circuit models fitted by ZSimpWin. The A and B models (Fig. 9d1 and d2) are often used to simulate the electrode interface structure of the initial and long-term immersion coatings [49–52], respectively (solution resistance R_s, coating resistance R_c, charge transfer resistance R_{ct}, constant phase element representing the coating capacitance Q_c, and double-layer capacitance Q_{dl}). During the initial immersion, the low-frequency impedance modulus values ($|Z|_{0.01 \text{ Hz}}$) of EP, BS/EP, and CBD/EP coatings are almost the same, which are 3.89×10^{11}, 2.07×10^{11}, and 3.31×10^{11} Ω cm^2, respectively. And the corresponding Nyquist plots all show a single capacitance characteristic, indicating that the three kinds of coatings are pure shielding layers. Model A has been used to fit the EIS results in this stage. Table 2 shows that they have higher coating resistance (R_c) and lower coating capacitance (Q_c). With the increase in immersion time to 36 days, the $|Z|_{0.01 \text{ Hz}}$ of BS/EP coating decreases to 1.713×10^{10} Ω cm^2. The Nyquist diagram shows two capacitance characteristics, and R_{ct} and Q_{dl} are introduced to further study the corrosion behavior. The appearance of R_{ct} and Q_{dl} components shows that the coating has been infiltrated and delaminated, and trace corrosive media may reach the interface of the coating substrate [53, 54]. For EP and CBD/EP coatings, the $|Z|_{0.01 \text{ Hz}}$ values of EP and CBD/EP coatings were kept at 2.09×10^{11} and 1.77×10^{11} Ω cm^2 after immersion for 36 days. At this stage, model B is used to fit the EIS results. With the further increase in immersion time, $|Z|_{0.01 \text{ Hz}}$ and the arc radius of Nyquist plot of all samples decreased gradually. Compared with other coatings, the CBD/EP coating shows a larger semicircular diameter on the Nyquist plot, which also shows that the coating has an excellent corrosion resistance [55]. After soaking for 155 d, it can be seen in the figure that the impedance modulus values of EP and BS/EP have decreased significantly, to 8.23×10^9 and 1.26×10^9 Ω cm^2, respectively, while the impedance modulus of CBD/EP is still as high as 1.35×10^{11} Ω cm^2.

The change of R_c, Q_c, and R_{ct} obtained by fitting the data is shown in Table 2. Generally, the size of R_c and Q_c is related to the impermeability and the barrier performance of the coating. The larger the R_c value, the better the impermeability of the coating; the smaller the Q_c value, the better the barrier property of the coating [46, 53]. Due to the erosion of corrosion medium, the R_c value of pure EP coating decreased to 1.942×10^{10} Ω cm^2 after 155 days. However, the R_c value of CBD/EP coating reaches 6.07×10^{10} Ω cm^2, which is higher than that of EP coating, indicating that CBD/EP coating can effectively restrain the penetration of corrosion medium. The Q_c value of CBD/EP coating (5.989×10^{-11} S s^n cm^{-2}) is less than that of EP coating (7.107×10^{-11} S s^n cm^{-2}), which indicates that the coating has a strong waterproof and invading ability and a desirable anticorrosion performance as it is consistent with the
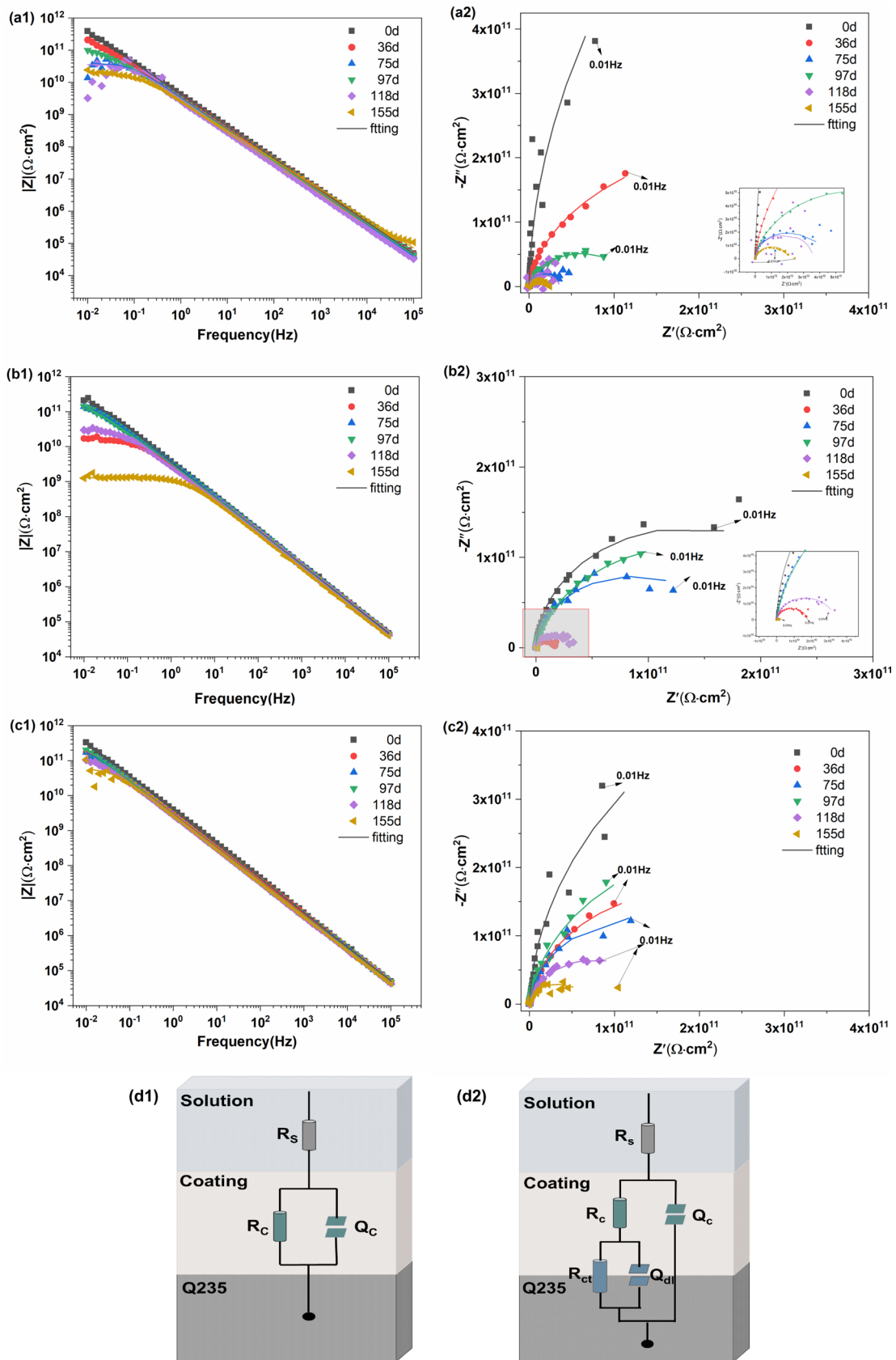
**Fig. 9** Impedance plots of **a1**, **a2** EP; **b1**, **b2** BS/EP; and **c1**, **c2** CBD/EP coatings immersed in 3.5 wt% NaCl solution for 155 d. Inserted the equivalent electrical circuits (model A **d1** and model B **d2**) used to fit the EIS data of coatings

Table 2 Electrochemical parameters extracted from EIS data of the EP, BS/EP, and CBD/EP immersed in 3.5 wt% NaCl solution for 155 d; the data are normalized to the total surface area (4.9 cm^2)

Sample	Time (day)	R_s	Q_c (S s^n cm^{-2})	n_c	R_c (Ω cm^2)	Q_{dl} (S s^n cm^{-2})	n_{dl}	R_{ct} (Ω cm^2)
EP	0	0.01	3.859×10^{-11}	0.99	2.623×10^{12}	–	–	–
	36	0.01	4.77×10^{-11}	0.98	1.816×10^{11}	3.873×10^{-11}	1.00	2.207×10^{11}
	75	0.02	4.861×10^{-11}	0.98	3.991×10^{10}	1.727×10^{-9}	1.00	4.998×10^{10}
	97	0.01	5.197×10^{-11}	0.97	4.762×10^{10}	3.815×10^{-11}	0.76	7.565×10^{10}
	118	0.01	5.003×10^{-11}	1.00	5.542×10^{9}	3.052×10^{-12}	1.00	3.019×10^{10}
	155	0.01	7.107×10^{-11}	0.91	1.942×10^{10}	1.112×10^{-13}	0.89	1.376×10^{9}
BS/EP	0	0.01	4.376×10^{-11}	0.98	2.741×10^{11}	–	–	–
	36	0.01	4.359×10^{-11}	0.99	1.253×10^{9}	2.485×10^{-11}	0.53	1.697×10^{10}
	75	0.01	4.337×10^{-11}	0.99	1.196×10^{10}	1.329×10^{-11}	0.83	1.625×10^{11}
	97	0.01	4.322×10^{-11}	0.99	2.967×10^{9}	1.694×10^{-11}	0.66	3.061×10^{11}
	118	0.01	4.806×10^{-11}	0.98	1.494×10^{9}	2.089×10^{-11}	0.71	3.004×10^{10}
	155	0.01	5.560×10^{-11}	0.98	9.347×10^{8}	1.820×10^{-10}	0.86	3.680×10^{8}
CBD/EP	0	0.01	4.263×10^{-11}	0.98	1.087×10^{12}	–	–	–
	36	0.01	4.152×10^{-11}	0.99	8.659×10^{7}	1.573×10^{-11}	0.78	3.903×10^{11}
	75	0.01	3.962×10^{-11}	0.99	1.400×10^{7}	1.936×10^{-11}	0.86	2.813×10^{11}
	97	0.01	5.798×10^{-11}	0.96	3.387×10^{11}	6.894×10^{-11}	1.00	1.385×10^{11}
	118	0.01	6.182×10^{-11}	0.96	6.095×10^{10}	2.087×10^{-11}	0.48	1.250×10^{11}
	155	0.01	5.989×10^{-11}	0.96	6.07×10^{10}	1.17×10^{-9}	1.00	4.459×10^{10}

water absorption test results in Fig. 7. R_{ct} is usually used to describe the corrosion rate and reflects the kinetics of the electrochemical reaction at the interface [15]. For EP and BS/EP coatings, the R_{ct} value decreased during the immersion process, but increased briefly in the middle stage, which may be caused by the accumulation of corrosion products. For the CBD/EP coating, the overall R_{ct} remains the highest and the most stable during the immersion process. It displays the highest and most stable R_{ct} value after 155 days of immersion, which further proves that the addition of CBD filler greatly improves the corrosion resistance of the coating.

$|Z|_{0.01\ Hz}$ can directly reflect the corrosion resistance [56, 57]. Throughout the soaking period, $|Z|_{0.01\ Hz}$ of EP and BS/EP samples quickly decreased from 3.89×10^{11} to 8.23×10^{9} and 2.07×10^{11} to 1.26×10^{9} Ω cm^2, respectively (Fig. 10), indicating a rapid decline of their corrosion resistances. The reason is that the pores of epoxy resin by the volatilization of its own solvent and the cracks by the incompatibility of the interface between BS/EP (Fig. 5c1 and c2) would become the fast channel of aggressive particles, and the corrosion medium would diffuse rapidly in these coatings during immersion (Fig. 6b), which is consistent with the results in the literature [58]. However, $|Z|_{0.01\ Hz}$ of CBD coating fluctuates slightly around a relatively high value after a slight decrease, which may be due to the strong chemical bonding between the modified filler interface and epoxy resin, as well as the hydrophobic properties near the interface by CeO$_2$ and PDA/GPTMS. Generally speaking, EIS analysis shows that the anticorrosion performance of CBD/EP hybrid coating is better than that of EP and BS/EP coatings, and the chemical
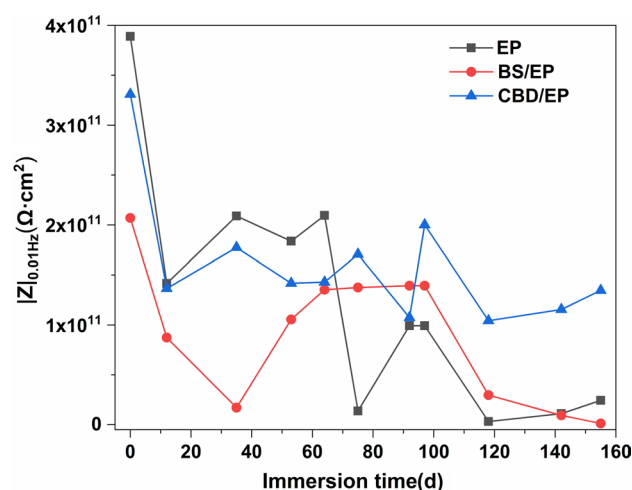
Fig. 10 Variation of $|Z|_{0.01\ Hz}$ of EP, BS/EP, and CBD/EP coating immersed in 3.5 wt% NaCl solution for different time

modification of PDA and GPTMS greatly improves the protective performance of CBD/EP coating.

When the corrosion medium reaches the surface of the metal substrate, an electrochemical reaction will occur, resulting in accumulation of corrosion products and the detachment of the coating from the substrate, which could cause changes in phase angle. So, the phase angle change is also a parameter (breakpoint frequency f_b) to assist in judging the internal change process of the coating. f_b refers to the frequency when the phase angle is $-45°$. It is always employed to evaluate the micro-delamination between coating and substrate. The earlier the breakpoint frequency

occurs and the higher the value, the earlier and faster the coating peels off [59, 60]. It can be seen from the phase angle diagram of Fig. 11a and b that it has the same downward trend as the impedance modulus. From Fig. 11a–c, the f_b values of these coatings at different soaking times can be obtained and plotted as Fig. 11d. And the f_b value of the BS/EP coating appears earliest and rapidly increases in the later stage of immersion, indicating that the coating is the first to peel off, and the peeling rate is also the fastest. However, the f_b value of CBD/EP coating only starts to appear after soaking for about 120 days and increases at a very small rate. The results show that compared with other coatings, the adhesion between CBD coating and metal substrate is the strongest, and it is not easy to peel off. In the adhesion test (Fig. 6), the adhesion of CBD has the highest value, corresponding to the change of breakpoint frequency.

3.5 Protective Mechanism of Basalt Scales/Epoxy Composite Coatings Modified by Cerium Dioxide and Polydopamine

Excellent physical shielding property is important to ensure long-term protection ability of the coating [61]. Based on the data above, the corrosion protection mechanism of the coatings was be analyzed, the schematic diagram is exhibited in Fig. 12. In the EP coating, due to its own defects, corrosion ions penetrated into the coating, causing corrosion to occur. In the BS/EP coating, because the density (2 g/cm³) of basalt is much higher than that of epoxy resin, the position of BS inside the coating layer was concentrated in the next layer. And the filler is physically combined with the epoxy resin to increase the gap between the interfaces. The defect becomes a fast passage for water and erosive ions, which causes corrosion to occur quickly. However, the corrosion resistance of the modified CBD/EP coating has been greatly improved, mainly from the following three aspects:

The surface activation treatment of BS and the deposition of CeO_2 can improve the mechanical bonding strength
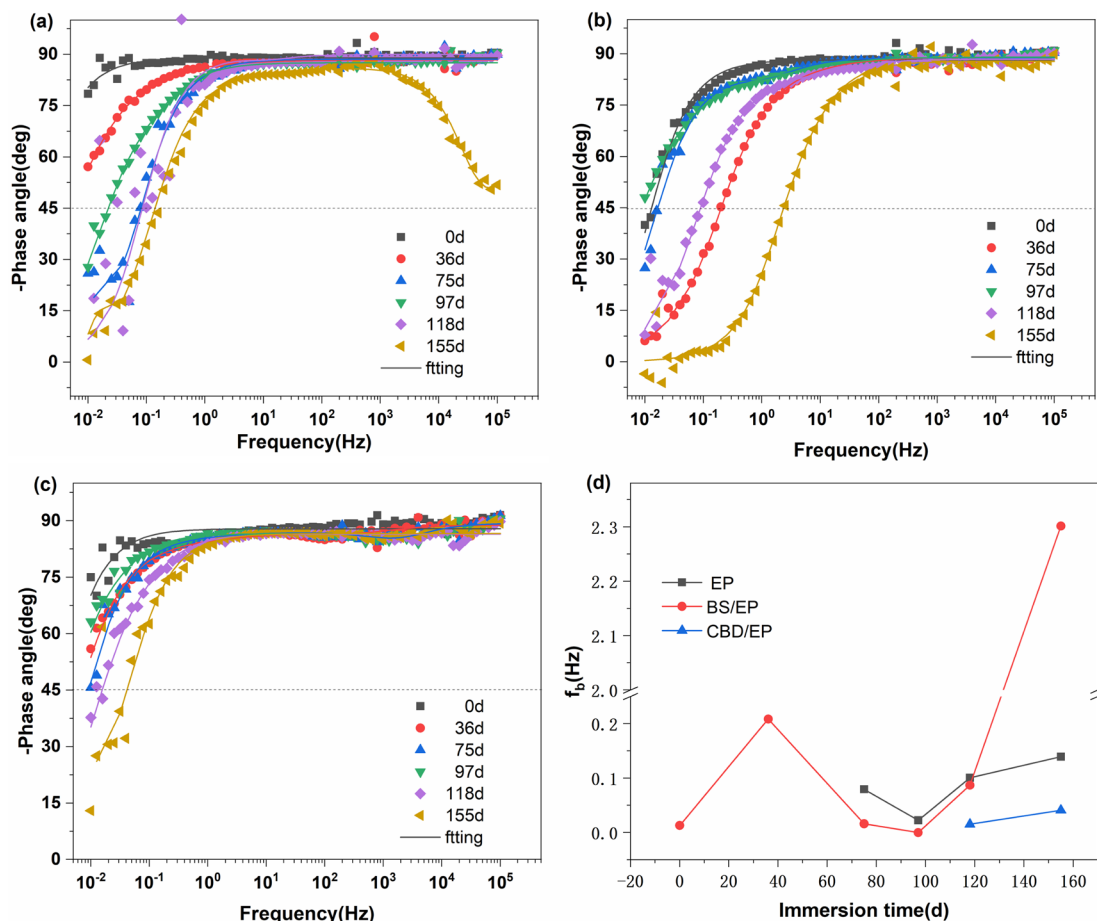

Fig. 11 Phase angle curves of **a** EP; **b** BS/EP and **c** CBD/EP coatings immersed in 3.5 wt% NaCl solution for 155 d. **d** Change curve of breakpoint frequency (f_b) with soaking time
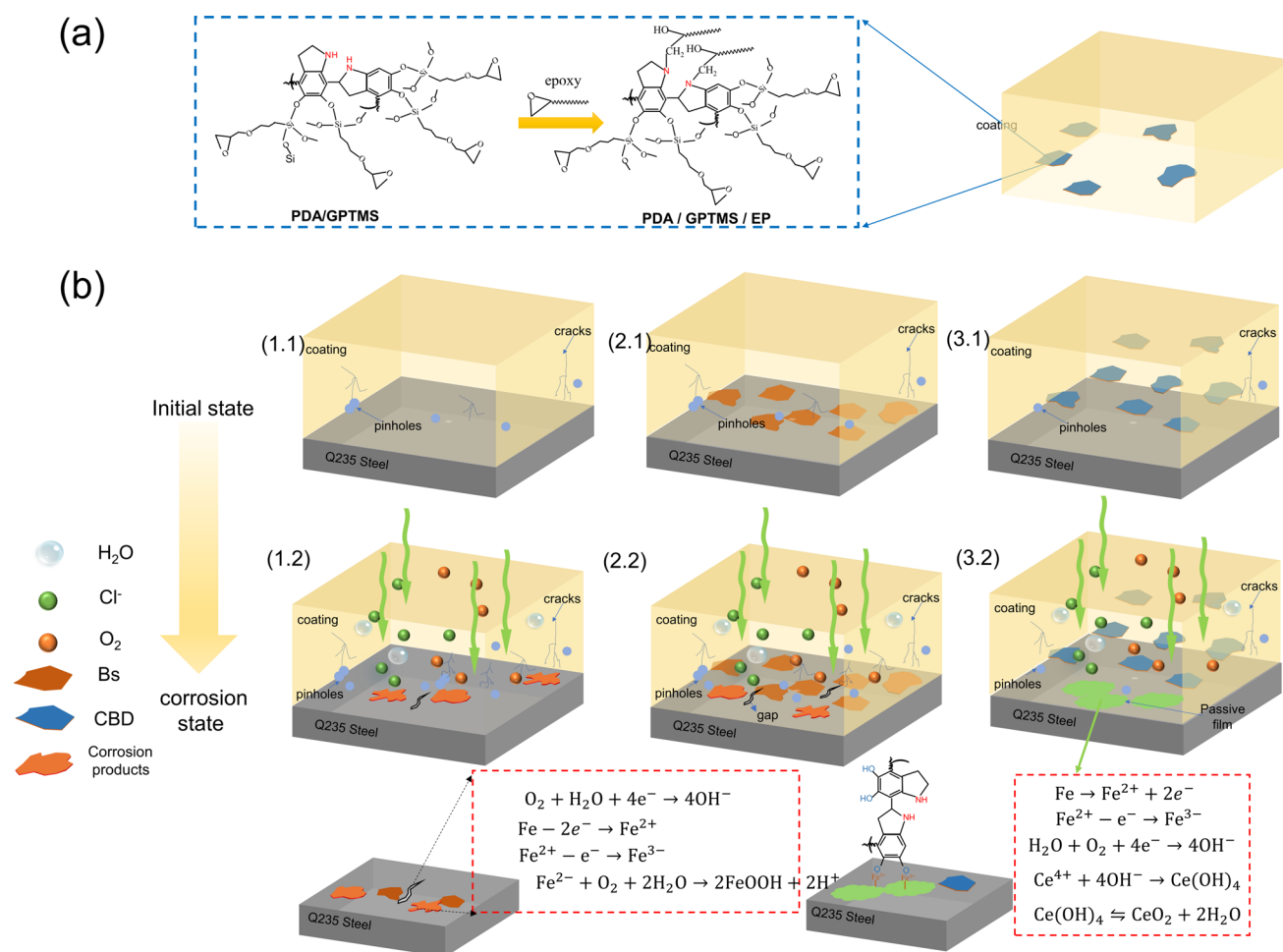
Fig. 12 Illustration of covalent binding of modified basalt scales (CBD) to epoxy resin **a**. The schematic diagram of corrosion mechanism for **b** (1.1, 1.2) pure EP, **b** (2.1, 2.2) BS/EP, and **b** (3.1, 3.2) CBD/EP

between basalt scales and epoxy resin. The secondary functionalization treatment changed the interfacial binding between basalt scales and epoxy resin from weak binding force to covalent bond. For example, the covalent chemical bonding was formed between dopamine (–NH₂) and EP polar functional group (epoxy group) (Fig. 12a). The dispersion of fillers in the coating is improved, the interface fast channel is greatly reduced, maximizing the maze effect.

After secondary functionalization (PDA/GPTMS), a large number of chain polymers were grafted onto the surface of BS, and the deposited CeO_2 enhanced the hydrophobicity near the interface. And the chemical bonding between dopamine/GPTMS and EP polar functional groups enhances the non-polarity of the coating near the interface, which makes the coating more hydrophobic and the transport of water in the coating more difficult [62].

CeO_2 has the characteristics of non-toxic and harmless, strong corrosion resistance and can form its hydroxide in a wide range of pH. Nano-CeO_2 dissolves in water

due to Gibbs–Thomson effect to produce Ce^{4+} cations. Ce^{4+} migrates to the coating/metal interface and reacts with hydroxyl groups in the cathode region of the metal surface as shown below (Fig. 12b) to form a dense protective film to prevent further corrosion [63]. What is more, PDA can also form a passivation layer on the surface of steel through catechol−Fe^{3+} coordination bond to delay the further corrosion process [64, 65].

4 Conclusions

In this study, the interface modification of basalt/epoxy resin and the properties of the coating were studied. The modified basalt scales were added to the epoxy coating to prepare a corrosion resistant coating with excellent properties. The following conclusions can be drawn:

1. Basalt scales are activated by a simple and environmentally friendly air plasma method, which makes the surface of basalt scales rich in hydroxyl. The abundant Si–OH groups can enhance the interaction between the carrier and CeO_2, and promote the high dispersion of CeO_2 on the surface.

2. Cerium dioxide nanoparticles were deposited on the surface of plasmonic-activated basalt scales, and then re-functionalized with PDA and GPTMS to improve the compatibility between CBD hybrid materials and coating matrix, and improve the mechanical properties and barrier properties of CBD/EP coatings. The enhanced mechanical and barrier properties make the CBD/EP coating to possess durable anticorrosion performance, and the impedance modulus was maintained as high as $1.35 \times 10^{11} \ \Omega \ cm^2$ after soaking in 3.5% NaCl solution for 155 d.

3. The protection mechanism of CBD/EP coating is explored. The improvement of CBD/EP coating performance is mainly due to the uniform dispersion of basalt scales in the coating and the increase in interface strength, which enhances the shielding effect of the coating. When corrosion occurs, CeO_2 and PDA will act as cathodic and anodic inhibitors, respectively, to prevent further corrosion.

Declarations

Conflict of interest The authors state that there are no conflicts of interest to disclose.

References

[1] Y. Ye, D. Zhang, T. Liu, Z. Liu, W. Liu, J. Pu, H. Chen, H. Zhao, X. Li, J. Hazaed. Mater. **364**, 244 (2019)

[2] M. Liu, S. Li, H. Wang, R. Jiang, X. Zhou, Polym. Chem. **12**, 3702 (2021)

[3] S. Pradhan, S. Kumar, S. Mohanty, S.K. Nayak, Polym-Plast Tech. Mat. **58**, 498 (2019)

[4] I. Dehri, M. Erbil, Corros. Sci. **42**, 969 (2000)

[5] Z.B. Bao, Q.M. Wang, S.M. Jiang, J. Gong, C. Sun, Corros. Sci. **50**, 2372 (2008)

[6] B. Ramezanzadeh, S. Niroumandrad, A. Ahmadi, M. Mahdavian, M.H.M. Moghadam, Corros. Sci. **103**, 283 (2016)

[7] G.X. Gu, F. Libonati, S.D. Wettermark, M.J. Buehler, J. Mech. Behav. Biomed. **76**, 135 (2017)

[8] N. Zhao, M. Yang, Q. Zhao, W. Gao, T. Xie, H. Bai, ACS Nano **11**, 4777 (2017)

[9] Y. Jing, P. Wang, Q. Yang, Q. Wang, Y. Bai, Colloid. Surf. A **608**, 125625 (2021)

[10] R. Teijido, L. Ruiz-Rubio, A.G. Echaide, J.L. Vilas-Vilela, S. Lanceros-Mendez, Q. Zhang, Prog. Org. Coat. **163**, 106684 (2022)

[11] S. Pourhashem, F. Saba, J. Duan, A. Rashidi, F. Guan, E.G. Nezhad, B. Hou, J. Ind. Eng. Chem. **88**, 29 (2020)

[12] S.S. Yao, M.Z. Gao, Z.Y. Feng, F.L. Jin, S.J. Park, Korean J. Chem. Eng. **39**, 1952 (2022)

[13] J. Yan, J. Shi, P. Zhang, W. Tian, Y. Zhang, Z. Sun, Mater. Corros. **69**, 1669 (2018)

[14] Y. Yu, Y. Zhang, Y. Chen, Z. Xu, Geochim. Cosmochim. Acta **179**, 257 (2016)

[15] D. Borisova, D. Akçakayıran, M. Schenderlein, H. Möhwald, D.G. Shchukin, Adv. Funct. Mater. **23**, 3799 (2013)

[16] Q. Yue, L. Wu, J. Lv, A. Wang, R. Ding, Y. Wang, L. Yue, W. Gao, X. Li, X. Li, Z. Cao, Y. Wang, Q. Gao, P. Han, H. Yu, X. Zhao, T. Gui, X. Wang, Colloid Interface Sci. Commun. **45**, 100505 (2021)

[17] L. Luo, Q. Ma, Q. Wang, L. Ding, Z. Gong, W. Jiang, Coatings **9**, 154 (2019)

[18] H. Zheng, L. Liu, F. Meng, Y. Cui, F. Wang, Prog. Org. Coat. **153**, 106160 (2021)

[19] Z. Li, L. Liu, H. Zheng, F. Meng, F. Wang, Compos. Commun. **31**, 101134 (2022)

[20] Y. Shi, G. Zhang, Y. Sun, H. Zheng, Z. Li, J. Shangguan, J. Mi, S. Liu, P. Shi, Chin. J. Inorg. Chem. **37**, 1004 (2021)

[21] V. Manikandan, J.T. Winowlin Jappes, S.M. Suresh Kumar, P. Amuthakkannan, Compos. Pt. B -Eng. **43**, 812 (2012)

[22] H. Zheng, L. Liu, F. Meng, Y. Cui, Z. Li, E.E. Oguzie, F. Wang, J. Mater. Sci. Technol. **84**, 86 (2021)

[23] C.Y. Zhi, Y. Bando, T. Terao, C.C. Tang, H. Kuwahara, D. Golberg, Chem. Asian J. **4**, 1536 (2009)

[24] Q. Guo, T. Wang, T.C. Zhang, L. Ouyang, S. Yuan, Prog. Org. Coat. **174**, 107300 (2023)

[25] F. Meng, T. Zhang, L. Liu, Y. Cui, F. Wang, Surf. Coat. Technol. **361**, 188 (2019)

[26] V.V. Efanova, V.N. Belinskii, Mech. Compos. Mater. **30**, 308 (1994)

[27] C.H. Yu, A. Al-Saadi, S.J. Shih, L. Qiu, K.Y. Tam, S.C. Tsang, J. Phys. Chem. C **113**, 537 (2009)

[28] S. Wang, P.J. Chia, L.L. Chua, L.H. Zhao, R.Q. Png, S. Sivaramakrishnan, M. Zhou, G.S. Goh, R.H. Friend, A.T.S. Wee, P.K.H. Ho, Adv. Mater. **20**, 3440 (2008)

[29] S. Liu, X. Zhang, C. Wang, C. Yin, J. Rao, Y. Zhang, D. Losic J. Magnes. Alloy. **21**, 3440 (2022)

[30] C. Zhao, H. Zheng, Y. Sun, S. Zhang, J. Liang, Y. Liu, Y. An, Sci. Total. Environ. **640–641**, 243 (2018)

[31] D. Yu, J. Wang, W. Hu, R. Guo, Mater. Des. **129**, 103 (2017)

[32] B. Mingo, Y. Guo, R. Leiva-Garcia, B.J. Connolly, A. Matthews, A.C.S. Appl, Mater. Interfaces **12**, 30833 (2020)

[33] S.A. Umoren, A. Madhankumar, J. Mol. Liq. **224**, 72 (2016)

[34] Y. Sasikumar, A.M. Kumar, Z.M. Gasem, E.E. Ebenso, Appl. Surf. Sci. **330**, 207 (2015)

[35] S. Ameen, M. Shaheer Akhtar, H.K. Seo, H.S. Shin, Chem. Eng. J. **247**, 193 (2014)

[36] Q.X. Yue, J. Lv, X. Liang, Y.Y. Wang, R. Ding, Y. Li, J.H. Deng, P. Han, H. Yang, T.Z. Sun, L. Sun, J.P. Xian, X.Y. Wang, L. Kong, X.Y. Wang, H.B. Yu, X. Wang, T.J. Gui, W.H. Li, J. Taiwan Inst. Chem. Eng. **131**, 104156 (2022)

[37] J. Berriot, F. Lequeux, L. Monnerie, H. Montes, D. Long, P. Sotta, J. Non-Cryst. Solids **307–310**, 719 (2002)

[38] Y. Nie, B. Wang, G. Huang, L. Qu, P. Zhang, G. Weng, J. Wu, J. Appl. Polym. **117**, 3441 (2010)

[39] B. Zhong, Z. Jia, Y. Luo, D. Jia, F. Liu, Polym. Test. **58**, 31 (2017)

[40] F. Meng, L. Liu, W. Tian, H. Wu, Y. Li, T. Zhang, F. Wang, Corros. Sci. **101**, 139 (2015)

[41] W. Tian, L. Liu, F. Meng, Y. Liu, Y. Li, F. Wang, Corros. Sci. **86**, 81 (2014)

[42] Y. Li, Y. Ma, B. Zhang, B. Lei, Y. Li, Acta Metall. Sin. -Engl. Lett. **27**, 1105 (2014)

[43] T.M. Abbas, S.I. Hussein, J. Inorg. Organomet. Polym. Mater. **32**, 3788 (2022)

[44] Y. Situ, Y. Guo, W. Ji, D. Liu, D. Wei, H. Huang, J. Coat. Technol. Res. **18**, 999 (2021)

[45] A. Miszczyk, K. Darowicki, Prog. Org. Coat. **124**, 296 (2018)

[46] C.A. Xu, Z. Chu, X. Li, H. Fang, W. Zhou, Y. Hu, X. Chen, Z. Yang, Prog. Org. Coat. **183**, 107804 (2023)

[47] S. Wan, C.H. Miao, R.M. Wang, Z.F. Zhang, Z.H. Dong, Prog. Org. Coat. **129**, 187 (2019)

[48] C. Ding, Y. Tai, D. Wang, L. Tan, J. Fu, Chem. Eng. J. **357**, 518 (2019)

[49] B.M. Hryniewicz, F. Wolfart, P. Gómez-Romero, E.S. Orth, M. Vidotti, Electrochim. Acta **338**, 135842 (2020)

[50] J. Huang, Z. Li, B.Y. Liaw, J. Zhang, J. Power. Sources **309**, 82 (2016)

[51] W. Guo, J. Hu, Y. Ma, H. Huang, S. Yin, J. Wei, Q. Yu, Corros. Sci. **165**, 108366 (2020)

[52] L. Shen, Y. Li, W. Zhao, K. Wang, X. Ci, Y. Wu, G. Liu, C. Liu, Z. Fang, J. Mater, Sci. Technol. **44**, 121 (2020)

[53] C. Wang, S. Liu, M. Li, Z. Wang, H. Luo, W. Fan, Z. Liu, F. Liu, H. Wang, Langmuir **37**, 9439 (2021)

[54] I.K. Nwokolo, H. Shi, P.C. Uzoma, S. Ahmed, J. Li, F. Liu, Acta Metall. Sin. -Engl. Lett. **36**, 1893 (2023)

[55] E. Alibakhshi, A. Naeimi, M. Ramezanzadeh, B. Ramezanzadeh, M. Mahdavian, J. Alloy. Compd. **762**, 730 (2018)

[56] Y. Chen, B. Ren, S. Gao, R. Cao, J. Colloid Interface Sci. **565**, 436 (2020)

[57] M. Cheng, J. Liu, Y. Liu, H. Jiang, C. Li, S. Sun, S. Hu, Chem. Eng. J. **459**, 141532 (2023)

[58] J. Ding, H. Zhao, H. Yu, ACS Nano **16**, 710 (2022)

[59] M. Ramezanzadeh, B. Ramezanzadeh, G. Bahlakeh, A. Tati, M. Mahdavian, Chem. Eng. J. **408**, 127361 (2021)

[60] Y. Su, S. Qiu, J. Wei, X. Zhu, H. Zhao, Q. Xue, Chem. Eng. J. **426**, 131269 (2021)

[61] J. Chen, W. Zhao, Chem. Eng. J. **423**, 130195 (2021)

[62] B. Peng, Z. Yu, L. Chen, K. Liao, H. Chen, Y. Guo, Y. Liu, J. Appl. Polym. Sci. **139**, e52866 (2022).

[63] X. Liu, C. Gu, Z. Wen, B. Hou, Prog. Org. Coat. **115**, 195 (2018)

[64] H. Khosravi, R. Naderi, B. Ramezanzadeh, Mater. Today Chem. **27**, 101282 (2023)

[65] G. Cai, S. Xiao, C. Deng, D. Jiang, X. Zhang, Z. Dong, Corros. Sci. **178**, 109014 (2021)